

Chapter 7

Dynamics of Nanodroplets on Structured Surfaces

Markus Rauscher

Abstract Fluids on the nanoscale behave qualitatively different from macroscopic systems. This becomes particularly evident if a free liquid–liquid or liquid–gas interface is close to a solid surface such as in the case of nanodroplets. In contrast to macroscopic drops, hydrodynamic slip, thermal fluctuations, the molecular structure of the liquid, and the range of the intermolecular interactions are important for the structure and the dynamics of such open nanofluidic systems. After a review of the macroscopic modeling and behavior of nonvolatile droplets on structured substrates, we discuss the static and dynamic peculiarities on the nanoscale with special emphasis on theory. In particular we show that nanodroplets experience long-ranged lateral interactions with sharp surface features and that their free energy might be lower on a less wettable part of the substrate surface. A discussion of possible experiments for observing these phenomena is followed by a summary and an outlook.

7.1 Introduction

Droplets are a particularly fascinating manifestation of wetting phenomena which occur as a result of two fluid phases (e.g., a liquid and a gas or two immiscible liquids) coming into contact with a solid surface. And they are not only ubiquitous in our everyday life but also of tremendous technological importance—in many cases because their formation should be avoided or because they should be removed. But they can be also used for patterning surfaces. For this reason we have some intuition how macroscopic droplets on surfaces should behave. In this chapter we show that

M. Rauscher (✉)

Max-Planck-Institut für Intelligente Systeme, Stuttgart, Germany

Institut für Theoretische Physik IV, Stuttgart, Germany

e-mail: rauscher@is.mpg.de

our intuition fails on the nanoscale (see also [1–4]) and we discuss theoretical approaches to the dynamics of liquids on the nanoscale, simulation methods, and experimental options.

Speaking of droplets also means speaking about nonvolatile liquids: a drop of a volatile liquid sitting on a chemically and topographically homogeneous surface is unstable: it either evaporates or, if the vapor phase is supersaturated, it grows without bound (or until the vapor reservoir is depleted). As a consequence, wetting phenomena of nonvolatile liquids are much richer. For example, on a homogeneous surfaces in contact with a vapor phase one obtains a homogeneous liquid film of a certain thickness which grows in thickness as one approaches liquid–vapor coexistence [5,6], whereas a nonvolatile liquid can form droplets. And on structured substrates one even observes morphological transitions between different droplet shapes. Strictly speaking, nonvolatility is a question of time scale and in this chapter we assume that the time scale of evaporation is large as compared to the time scale of the motion of the nanodroplets.

In the following we speak about liquid droplets surrounded by a thin gas phase of negligible viscosity on an inert solid substrate. However, apart from the viscous dissipation in the second liquid phase, the results presented below can be generalized to a system of two immiscible liquids in a straightforward way.

The following Sect. 7.2 contains a review of the behavior of macroscopic droplets on chemically (Sect. 7.2.1) and topographically (Sect. 7.2.2) structured substrates, with particular focus on the aspects which are different on the nanoscale. In Sect. 7.3 the dynamics of nanodroplets on structured substrates is discussed. Section 7.3.1 gives a concise overview of the equilibrium dynamic density functional theory (DFT) and the effective interface model which describe the equilibrium properties of nanodroplets. A mesoscopic extension of hydrodynamics is presented in Sect. 7.3.2. In Sect. 7.3.3 several simulation methods applicable to nanofluidics are compared. The peculiar behavior of nanodroplets on topographically and chemically structured substrates is illustrated in Sects. 7.3.4 and 7.3.5, respectively. Section 7.3.6 discusses experiments which might be capable of observing the dynamics of nanodroplets on structured substrates. A summary and outlook can be found in Sect. 7.4.

7.2 Macroscopic Droplets

Throughout this section we assume that gravity has a negligible effect on the shape of the droplets, i.e., that the Bond number $\text{Bo} = \rho g L^2 / \gamma$ (with the mass density ρ , the gravitational acceleration g , the surface tension γ , and a characteristic length scale L) is small. For water droplets this would be the case for radii less than a millimeter (the capillary length of water is $L_{\text{cap}} = \sqrt{\gamma / (\rho g)} = 2.6 \text{ mm}$).

The equilibrium shape of nonvolatile macroscopic droplets on solid substrates is determined by interface energies [7]. Its free energy is given by

$$F = A_{\text{LG}} \gamma + A_{\text{LS}} \gamma_{\text{LS}} + A_{\text{SG}} \gamma_{\text{SG}}, \quad (7.1)$$

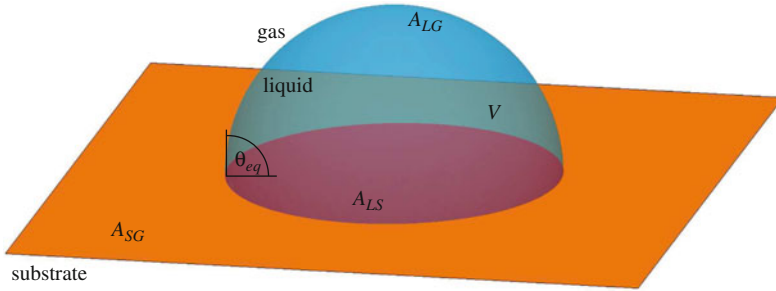


Fig. 7.1 A macroscopic liquid droplet of fixed volume V on a flat and homogeneous substrate forms a hemispherical cap with. The angle θ_{eq} between the liquid–gas interface and the substrate surface is given by Young’s law, i.e., it is determined by the interface tensions γ of the liquid–gas interface A_{LG} , γ_S of the liquid–substrate interface A_{LS} , and γ_{SG} of the substrate–gas interface A_{SG} . Here $\gamma_{LG} = \gamma_{SG}$ and therefore $\theta_{\text{eq}} = 90^\circ$

with the area of the liquid–substrate interface A_{LS} , the area of the liquid–gas interface A_{LG} , and the area of the substrate–gas interface A_{SG} . The corresponding interface tensions are γ_{LS} , $\gamma = \gamma_{LG}$, and γ_{SG} , respectively. Fixing the total substrate area $A = A_{SG} + A_{LS}$ as well as the liquid volume V and minimizing F with respect to the shape of the liquid–gas interface lead to Young’s law for the equilibrium contact angle θ_{eq}

$$\cos \theta_{\text{eq}} = \frac{\gamma_{SG} - \gamma_{LS}}{\gamma} \quad (7.2)$$

and to the Euler–Lagrange equation

$$2\gamma H_{LG} + p = 0, \quad (7.3)$$

which states that the Laplace pressure is constant on the liquid–gas interface. H_{LG} is the mean curvature of the liquid–gas interface and p is the hydrostatic pressure in the droplet. The pressure p is the Lagrange multiplier which fixes the liquid volume V . Therefore the liquid–gas interface has a constant mean curvature and in the case of a flat substrate (7.3) together with Young’s equation (7.2) as boundary condition leads to a spherical cap as shown in Fig. 7.1 for the example of $\theta_{\text{eq}} = 90^\circ$.

7.2.1 Chemically Structured Substrates

On homogeneous substrates the free energy of the droplet is independent of the position of the droplet. This is also the case for droplet positions on a homogeneous part of a substrate, e.g., on a hydrophilic or on a hydrophobic patch of a chemically structured substrate, or on a flat region of a topographically structured substrate.

On a chemically heterogeneous substrate this is no longer true. In this case, the contributions from the substrate surface to the free energy in (7.1) have to be replaced by an integral over the substrate surface

$$F = A_{LG} \gamma + \int_{A_{LS}} \gamma_{LS}(\mathbf{r}) dA + \int_{A_{SG}} \gamma_{SG}(\mathbf{r}) dA. \quad (7.4)$$

On a chemically heterogeneous substrate the interface energies $\gamma_{LS}(\mathbf{r})$ and $\gamma_{SG}(\mathbf{r})$ depend on the position \mathbf{r} on the surface. If a droplet is positioned on a chemical step between a hydrophilic region and a hydrophobic region, it will move to hydrophilic side and it stops as soon as the complete liquid–substrate interface rests on the hydrophilic part [8] (unless the initial shape of the droplet is far from equilibrium which can result in the droplet being situated completely on the more hydrophobic part of the surface after the initial shape relaxation where it will simply stay [9]). On a surface with a continuous variation of the wetting properties (a so-called chemical gradient), drops can move over distances greater than their diameter [10–12].

Chemically structured substrates have been suggested as an alternative to closed channels for microfluidic applications. This approach is based on the macroscopic observation that nonvolatile liquids on a hydrophobic substrate patterned with hydrophilic stripes will stay on these so-called chemical channels [13, 14] even if driven along the channels [15–17].

7.2.2 Topographically Structured Substrates

As mentioned above, the free energy of a droplet is independent of the droplet position only if the substrate is homogeneous and flat. The free energy of a droplet on a topographically structured substrate is also given by (7.1); however, calculating the first variation of F with respect to the shape of the liquid–gas interface and the position of the three-phase contact-line is a nontrivial task. Finite element codes such as the SURFACE EVOLVER can be used to determine the equilibrium shape of droplets numerically [18]. Topographically structured substrates have many technological applications: roughness modifies the wetting properties leading to superhydrophilic (for $\theta_{eq} < 90^\circ$) or superhydrophobic (surfaces for $\theta_{eq} > 90^\circ$) surfaces (the first ones are suggested as anti-fogging coatings and the latter ones have self-cleaning properties) [19–22]. As a result gradients in the roughness are expected to induce the motion of droplets in the same way as the chemical gradients mentioned above [23].

Grooves in surfaces can guide liquids in a way similar to chemical channels [24–26]. This is based on the observation that droplets are pinned by edges on surfaces. It has been already observed by Gibbs [27] that at the edge the contact angle is ill defined as shown in Fig. 7.2. It can be measured with respect to either of the sides

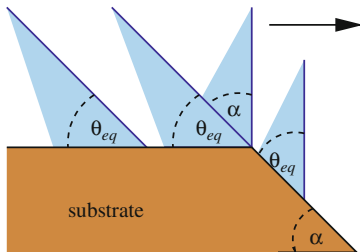


Fig. 7.2 The three-phase contact-line of a droplet approaching an edge in the substrate (here from *left to right*) advances only if the angle of the liquid–gas interface with the substrate is larger than the equilibrium contact angle θ_{eq} . At the edge the contact angle is ambiguous and in order to move down the slope of the edge it has to increase from θ_{eq} to $\theta_{eq} + \alpha$, with the angle of the slope α

of the edge. In order to overcome the edge the contact angle with the down-hill side of the edge has to be larger than the equilibrium contact angle θ_{eq} [28]. Actually it has to be even larger than the so-called advancing contact angle, which is larger than θ_{eq} . Even a rounded edge can pin a three phase contact line; however, the pinning strength depends on the edge shape [29]. Pinning at defects is the main reason for the difference of contact angle if the three phase contact line is receding (e.g., in dewetting) or advancing (e.g., for spreading droplets). Only recently it has become possible to directly measure the pinning strength of individual nanoscale defects [30].

Topographically structures can also trigger morphological phase transitions of the shape of droplets, e.g., between drops and filaments in rectangular grooves [24, 26]. And on fibers one observes a transition from a symmetric barrel shape for large volumes and small contact angles to an asymmetric clamshell shape for small volumes and large contact angles [31].

7.2.3 Dynamics

For radii larger than a micron the dynamics of nonvolatile liquid droplets is well described by macroscopic hydrodynamic equations. Here we focus on incompressible simple Newtonian liquids surrounded by a vapor or gas of negligible viscosity and density. On the micron-scale the Reynolds number $Re = \rho UL/\eta$ (with a characteristic velocity U and the liquid viscosity η) is much smaller than one and the liquid velocity $\mathbf{u}(\mathbf{r}, t)$ as well as the pressure $p(\mathbf{r}, t)$ can be determined by solving the Stokes equation

$$\nabla p = \eta \nabla^2 \mathbf{u} \quad (7.5)$$

together with the incompressibility condition

$$\nabla \cdot \mathbf{u} = 0. \quad (7.6)$$

For incompressible nonvolatile liquids the normal velocity $v = \hat{\mathbf{n}} \cdot \mathbf{u}$ of the moving liquid–gas interface is given by the component of the liquid velocity normal to the interface ($\hat{\mathbf{n}}$ denotes the outward normal vector at the liquid–gas interface). In the Monge parameterization $z = h(x, y, t)$ the nonlinearity of this kinematic condition becomes apparent:

$$\partial_t h = u_z - u_x \partial_x h - u_y \partial_y h \quad \text{at } A_{LG}. \quad (7.7)$$

At the surface of impermeable substrates the normal component of the liquid velocity vanishes. Macroscopically it is valid to assume that the tangential velocity is also zero [32]. With the substrate surface at rest this leads to a Dirichlet type boundary condition at the substrate interface

$$\mathbf{u} = 0 \quad \text{at } A_{LS}. \quad (7.8)$$

Here we assume that the viscosity and pressure of the gas phase are negligible such that the tangential forces on the liquid–vapor interface vanish and the normal component of the stress tensor is balanced by the Laplace pressure from (7.3). In summary we have

$$\boldsymbol{\sigma} \cdot \hat{\mathbf{n}} = 2\gamma H_{LG} \hat{\mathbf{n}} \quad \text{at } A_{LG}, \quad (7.9)$$

with the stress tensor of an incompressible Newtonian fluid

$$\sigma_{ij} = -p \delta_{ij} + \eta (\partial_j u_i + \partial_i u_j). \quad (7.10)$$

Up to the motion of the three-phase contact-line between liquid, gas, and substrate, the dynamics of a macroscopic droplet is well described by (7.5) to (7.10). Within these equations, the stress $\boldsymbol{\sigma}$ and also the dissipation in a moving three-phase contact-line diverges. As a consequence it should not move [5, 33] although everyday experience tells that it does [34]. This is an artifact of this macroscopic model.

7.3 Nanofluidics

On the nanoscale, phenomena which are either irrelevant or summarized in hydrodynamic boundary conditions come into play which lead to qualitative changes in the equilibrium properties as well as in the dynamics of liquids. These are on one hand the finite range of intermolecular forces, thermal fluctuations, and the molecular structure of the liquid which also strongly influence static wetting properties and on the other hand hydrodynamic slip which strongly influences the dynamics [1, 3, 4]. In the following we show how to augment the hydrodynamic equations presented in Sect. 7.2 such that they can be used to describe the dynamics

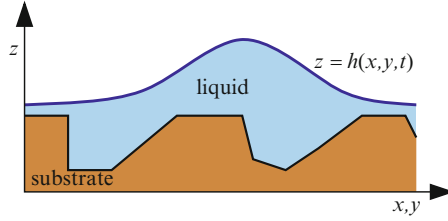


Fig. 7.3 For the clarity of the presentation, we consider a structured substrate aligned with the xy -plane and we assume that the liquid–gas interface can be parameterized by the Monge parameterization $z = h(x, y, t)$

of nanodroplets. Unfortunately it is not yet possible to include the effects of the molecular structure of the liquid into dynamical theories. The static molecular structure of liquids is well understood [35].

For the clarity of the presentation, in the following we consider a (structured) substrate aligned with the xy -plane of our coordinate system and we assume that the liquid–gas interface has no overhangs such that we can use the Monge parameterization $z = h(x, y, t)$ as illustrated in Fig. 7.3.

7.3.1 Density Functional Theory

Great progress has been made in understanding wetting phenomena by using the classical DFT for inhomogeneous systems [36]. One can show that there exists a functional $\Omega[\rho]$ which is minimized by the equilibrium density distribution of a grand canonical ensemble of classical particles (i.e., a system of a given volume V in thermal and chemical equilibrium with a bath at a given temperature T and chemical potential μ). For a one-component system of indistinguishable particle this functional has the form

$$\Omega[\rho] = \mathcal{F}_{\text{id}}[\rho] + \mathcal{F}_{\text{ext}}[\rho] + \mathcal{F}_{\text{ex}}[\rho] - \mu \int_V \rho(\mathbf{r}) d^3r, \quad (7.11)$$

with the ideal gas part ($\Lambda = h/\sqrt{2\pi mk_B T}$ with the Planck constant h , the Boltzmann constant k_B , the molecular mass m is the thermal de Broglie wavelength)

$$\mathcal{F}_{\text{id}}[\rho] = k_B T \int_V \rho(\mathbf{r}) (\ln(\rho(\mathbf{r}) \Lambda^3) - 1) d^3r, \quad (7.12)$$

with the contribution due to an external potential $\Phi_{\text{ext}}(\mathbf{r})$ which also describes the substrate

$$\mathcal{F}_{\text{ext}}[\rho] = \int_V \rho(\mathbf{r}) \Phi_{\text{ext}}(\mathbf{r}) d^3r, \quad (7.13)$$

and with the so-called excess free energy $\mathcal{F}_{\text{ex}}[\rho]$ due to the intermolecular interactions.

The proof of existence of a classical DFT is non-constructive and $\mathcal{F}_{\text{ex}}[\rho]$ is only known exactly in two cases: for ideal gases ($\mathcal{F}_{\text{ex}}[\rho] = 0$) and for a one-dimensional system of hard particles [37]. But rather sophisticated functionals for hard-sphere systems are available [38, 39]. The advantage of these functionals is that they can even capture the molecular structure of the liquid such as layering effects near hard walls. We want to use the DFT results to understand not only the equilibrium properties of droplets but also their dynamics.

Unfortunately, it is not possible up to now to include effects of the molecular structure of the liquid into hydrodynamic theory. However, one can make significant progress by splitting the intermolecular interaction potential into a short-ranged, hard repulsive part and a long-ranged attractive part $\Phi_{\text{att}}(r)$. One effectively gets a system of hard spheres with soft attractions. If one further neglects short distance correlations in the liquid due to packing effects, one can use a local approximation for the hard sphere part of the density functional leading to

$$\mathcal{F}_{\text{ex}}[\rho] = \int_V \left(f_{\text{HS}}(\rho(\mathbf{r})) + \frac{1}{2} \rho(\mathbf{r}) \int \Phi_{\text{att}}(|\mathbf{r} - \mathbf{r}'|) \rho(\mathbf{r}') d^3 r' \right) d^3 r, \quad (7.14)$$

with the Carnahan–Starling expression $f_{\text{HS}}(\rho) = k_{\text{B}} T \rho \left(\ln(\rho \Lambda^3) - 1 + \frac{4\eta - 3\eta^2}{(1-\eta)^2} \right)$ and the packing fraction $\eta = \frac{4\pi}{3} R^3 \rho$ [35]. The (effective) particle radius R depends on the temperature and on details of the repulsive part of the intermolecular interactions.

In a liquid film the liquid density rises from zero right at the substrate surface to the bulk liquid density ρ_{L} within a few molecular diameters. Far from critical points the liquid–gas interface has a width of the order of a few molecular diameters. Within this interface the density changes gradually from the bulk liquid density to the bulk gas density ρ_{G} .

On a mesoscopic length scale the density distribution of liquid molecules within a film of thickness h is reasonably well approximated by step-like profile

$$\rho_{\text{step}}(z, h) = \begin{cases} 0, & \text{for } z < 0 \\ \rho_{\text{L}}, & \text{for } 0 < z < h. \\ \rho_{\text{G}}, & \text{for } h < z \end{cases} \quad (7.15)$$

The density of a film of laterally varying thickness $h(x, y)$ is given by $\rho_{\text{step}}(z, h(x, y))$. Therefore, the density is parameterized by the film thickness $h(x, y)$ and the density functional in (7.11) reduces to a functional of $h(x, y)$, which is called effective interface Hamiltonian [6, 40]. If the curvature of the liquid–gas interface H_{LG} is small (i.e., if the radii of curvature are large as compared to the range of the intermolecular interactions), the surface tension can be written in a local approximation leading to

$$\mathcal{H}[h] = \int \left(\gamma \sqrt{1 + (\nabla h)^2} + \omega(x, y, h(x, y)) - p h(x, y) \right) dx dy. \quad (7.16)$$

The so-called effective interface potential $\omega(x, y, z)$ describes the effective interaction between the liquid–substrate and the liquid–gas interface and the pressure p is proportional to the chemical potential μ at liquid–gas coexistence. Far from the substrate surface $\omega(x, y, z)$ goes to zero. The Euler–Lagrange equation corresponding to (7.16)

$$2\gamma H_{LG} + \Pi(x, y, z) + p = 0 \quad \text{at} \quad z = h(x, y), \quad (7.17)$$

with the disjoining pressure $\Pi(x, y, z) = \partial\omega(x, y, z)/\partial z$, balances the pressure, the Laplace pressure, and the disjoining pressure at the liquid–gas interface.

Although strictly speaking the DFT is only valid for grand canonical systems, it can be used to describe nonvolatile liquids (i.e., canonical ensembles) if one interprets the pressure in (7.17) as the Lagrange multiplier which fixes the liquid volume. In this sense (7.17) generalizes (7.3) to the nanoscale.

Assuming additive and pairwise interactions, the disjoining pressure can be expressed in terms of the attractive part Φ_{att} of the liquid–liquid interaction potential and the liquid–substrate interaction potential Φ_{sub} as an integral over the substrate volume [41]

$$\Pi(\mathbf{r}) = \int_{\text{substrate}} \left(\rho_L^2 \Phi_{\text{att}}(\mathbf{r} - \mathbf{r}') - \rho_L \rho_S(\mathbf{r}) \Phi_{\text{sub}}(\mathbf{r}) \right) d^3 r. \quad (7.18)$$

The external potential in (7.13) is given by $\Phi_{\text{ext}}(\mathbf{r}) = \int_{\text{subs.}} \rho_S(\mathbf{r}) \Phi_{\text{sub}}(\mathbf{r} - \mathbf{r}') d^3 r'$, with the substrate density $\rho_S(\mathbf{r})$. For inhomogeneous substrates the substrate density depends on the position in the substrate. Assuming power law potentials $\sim r^{-\alpha}$ each integration increases the exponent by one. Therefore the contribution from the bulk of the substrate (after integration with respect to x , y , and z) is $\sim r^{-\alpha+3}$ and therefore the one with the largest exponent and the longest interaction range. In experiments the wetting properties of surfaces are often modified by thin coatings. The contribution of such a thin coating to the disjoining pressure is then calculated by effectively integrating with respect to x and y only such that it is $\sim r^{-\alpha+2}$, i.e., much weaker and shorter in range than the contribution from the bulk. Thick liquid films therefore only “see” the bulk of the underlying substrate.

For Lennard-Jones type interaction potentials (the long-ranged attractive part of which is given by (non-retarded) van-der-Waals type dispersion forces) the effective interface potential of a homogeneous and flat substrate have the form

$$\omega(z) = \frac{A_H}{z^2} + \frac{B}{z^3} + \frac{C}{z^8}, \quad (7.19)$$

with the Hamaker constant A_H and $C > 0$. $A_H > 0$ and $B < 0$ correspond to the rather generic case of a substrate with a first order wetting transition and $A_H < 0$ and $B = 0$ to a substrate that exhibits critical wetting (see Fig. 7.4). In (7.18) one can generate

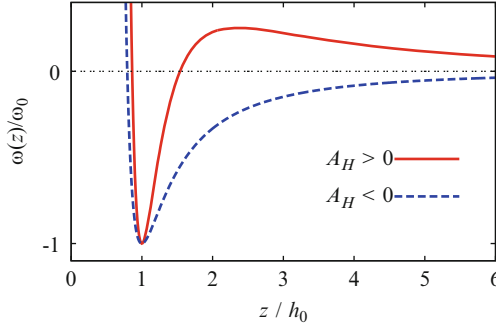


Fig. 7.4 The effective interface potential $\omega(z)$ of a flat and homogeneous partially wetting substrate as a function of the distance z from the substrate surface has a minimum of depth $-\omega_0$ at $z = h_0$. Shown are two examples, one with positive Hamaker constant $A_H > 0$ (*full red line*) and one with negative Hamaker constant $A_H < 0$ (*dashed blue line*)

the term proportional to B by assuming a very thin layer of a different material at the substrate surface. In real systems this term is also generated by the atomistic structure of the substrate and therefore it is rather generic [42]. For partially wetting substrates $\omega(z)$ has a minimum at $z = h_0$ of depth $\omega_0 = -\omega(h_0)$. By integrating the Euler–Lagrange equation (7.17) for a drop of infinite size (i.e., for $p = 0$) one can show that $\gamma_{SG} - \gamma_{LS} = \gamma - \omega_0$ and therefore

$$\cos \theta_{\text{eq}} = 1 - \frac{\omega_0}{\gamma}. \quad (7.20)$$

The deeper the minimum of $\omega(z)$, the larger the macroscopic equilibrium contact angle θ_{eq} . $\omega_0 > 2\gamma$ corresponds to complete drying and $\omega_0 = 0$ (i.e., if $\omega(z)$ does not have a minimum at finite distance from the substrate) corresponds to complete wetting $\theta_{\text{eq}} = 0^\circ$.

Figure 7.5 shows the disjoining pressure for van-der-Waals type dispersion forces in the vicinity of a straight topographic step of height $s = 3h_0$ in an otherwise homogeneous substrate [43]. The material parameters in (a) and (b) are chosen such that the effective interface potential far from the step ($|x| \rightarrow \infty$) is given by the solid and dashed line in Fig. 7.4, respectively. The system is translationally invariant in y -direction. For $A_H > 0$ (Fig. 7.5a) the disjoining pressure is positive for large z . Far from the step, as a function of z there is a local maximum at a distance of about $3h_0$ from the surface and there is a local minimum at a distance of about $1.15h_0$. As one approaches the edge from the left, the minimum becomes deeper and the maximum higher. For $A_H < 0$ (Fig. 7.5b) the disjoining pressure is negative for large z . Far from the step, as a function of z there is only a minimum at a distance of about $1.2h_0$ from the substrate. As one approaches the step from the left, the minimum becomes more shallow.

Figure 7.5 clearly shows that on the nanoscale the topographic step induces a lateral variation of the disjoining pressure. For van-der-Waals type forces and for large $|x|$ (and finite z) we have $\Pi(x, z) - \Pi_{\text{hom}}(z) \sim A_h s/x^4$, with the disjoining

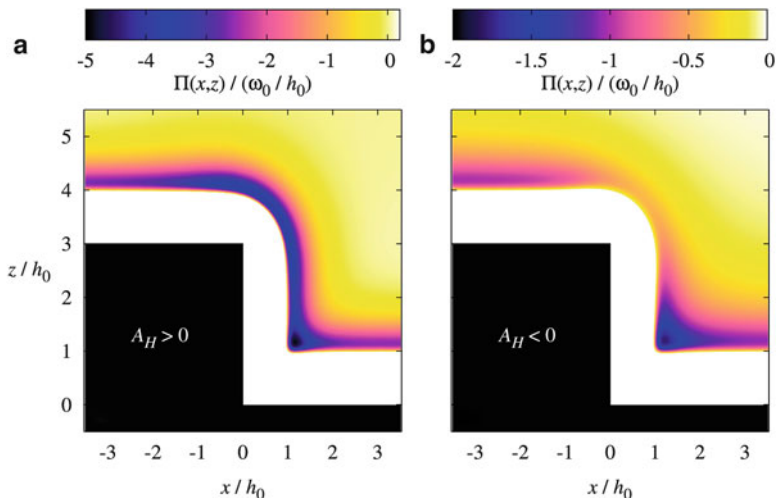


Fig. 7.5 The disjoining pressure $\Pi(x, z)$ at a straight topographic step of height $s = 3h_0$ which is aligned with the y -axis for (a) $A_H > 0$ and (b) $A_H < 0$. The parameters are chosen such that the corresponding effective interface potentials far from the step (i.e., for $x \rightarrow \infty$) are those shown in Fig. 7.4. The substrate is shown in black. In the white region next to the substrate the disjoining pressure is extremely large. The upper boundary of the white region roughly corresponds to the contour line $\Pi(x, z) = 0$. In (a) the disjoining pressure is positive for large z and in (b) it is negative

pressure of the flat and homogeneous substrate $\Pi_{\text{hom}}(z) = \lim_{|x| \rightarrow \infty} \Pi(x, z)$. As we will see later, a nanodroplet placed in the vicinity of such a step will experience a lateral force and the sign of this force depends on the sign of A_H .

7.3.2 Mesoscopic Hydrodynamics

Equation (7.17) not only allows to calculate the equilibrium shape of nanodroplets but it can be also used to generalize the stress boundary condition for the Stokes flow (7.9): the normal component of the stress tensor in the liquid is balanced by the Laplace pressure and the disjoining pressure

$$\boldsymbol{\sigma} \cdot \hat{\mathbf{n}} = (2\gamma H_{\text{LG}} + \Pi) \hat{\mathbf{n}} \quad \text{at } A_{\text{LG}}. \quad (7.21)$$

Equation (7.21) effectively takes into account the long-ranged nature of intermolecular interactions. And it has been shown, that, e.g., dewetting dynamics of thin films can be modeled quantitatively using this approach [44, 45].

Thermal fluctuations can be phenomenologically modeled by a randomly fluctuating stress tensor $\mathbf{S}(\mathbf{r}, t)$ of zero mean $\langle \mathbf{S}(\mathbf{r}, t) \rangle = 0$ and correlation function [46]

$$\langle S_{ij}(\mathbf{r}, t) S_{lm}(\mathbf{r}', t') \rangle = 2 \eta k_B T \delta(\mathbf{r} - \mathbf{r}') \delta(t - t') (\delta_{il} \delta_{jm} + \delta_{im} \delta_{jl}). \quad (7.22)$$

The amplitude of the noise is dictated by the fluctuation dissipation theorem. This form proposed can also be derived from the deterministic Boltzmann equation in a long-wave approximation [47]. Noisy hydrodynamical equations have been discussed in the context of turbulence in randomly stirred liquids [48, 49] as well as for the onset of instabilities in Rayleigh–Bénard convection [50] and Taylor–Couette flow [51]. Since the right-hand side of the Stokes equation (7.5) is the divergence of the deviatoric part of the stress tensor, we get

$$\nabla p = \eta \nabla^2 \mathbf{u} + \nabla \cdot \mathbf{S}. \quad (7.23)$$

It has been shown that including thermal fluctuations is crucial for understanding spinodal dewetting of thin films [52], i.e., when a soft mode is present in the system, or in order to overcome energetic barriers. If there is no barrier (or if it is too high to be overcome by thermal fluctuations) and if there is no soft mode, the main effect of thermal fluctuations in a droplet or in a thin film is capillary waves, which can lead to an effective steric repulsion of the liquid–gas interface from the wall, for a review see [53]. This effect can be summarized into the effective interface potential such that in the following we will not explicitly discuss the influence of thermal fluctuations on the dynamics of nanodroplets.

Slip at the liquid–substrate interface is a result of structural changes in a liquid in the direct vicinity of an interface. These structural changes lead to changes in the rheology of the liquid. Another reason for slip is the weak coupling of a liquid to a hydrophobic substrate. If one extrapolates the flow profile in a droplet (e.g., $u_x(z)$ on a flat substrate located in the xy -plane) to the substrate surface, one sometimes finds that the height z at which the velocity goes to zero is negative, i.e., at a point within the substrate. The depth b at which $u_x(b) = 0$ is called the slip length and for simple liquid it is usually on the nanometer scale [32]. Therefore it is irrelevant for macroscopic systems. However, it has been shown that hydrodynamic slip strongly influences dewetting phenomena [54–56].

On the length scale of a few inter-atomic distances and above, slip can be effectively described by replacing (7.8) by a Navier slip boundary condition

$$u_{\perp} = 0 \quad \text{and} \quad \mathbf{u}_{\parallel} = b \nabla_{\perp} \mathbf{u}_{\parallel} \quad \text{at} \quad A_{\text{LS}}. \quad (7.24)$$

Here $u_{\perp} = \mathbf{u} \cdot \hat{\mathbf{n}}_{\text{S}}$ denotes the component of the flow field perpendicular to the substrate surface (which has to be zero for impermeable substrates) and $\mathbf{u}_{\parallel} = \mathbf{u} - u_{\perp} \hat{\mathbf{n}}_{\text{S}}$ the components (two in three dimensions) parallel to the substrate surface. $\nabla_{\perp} = \hat{\mathbf{n}}_{\text{S}} \cdot \nabla$ is the derivative in the direction normal to the substrate surface and $\hat{\mathbf{n}}_{\text{S}}$ denotes the normal vector to the substrate surface pointing into the liquid. The Navier slip boundary states that the slip velocity \mathbf{u}_{\parallel} is proportional to the shear stress in the direction parallel to the substrate surface $\sigma \cdot \hat{\mathbf{n}}_{\text{S}}$.

7.3.3 Simulation Methods

Equations (7.5), (7.6), (7.7), (7.21), and (7.24) form a nonlinear moving boundary value problem. Solving these equations is further complicated by the fact that the dynamics of nanodroplets is dominated by surface tension, which requires precise calculation of the curvature (i.e., of the second derivative) of the liquid–gas interface. In addition, the disjoining pressure is rather stiff (i.e., it has steep gradients) in the vicinity of the substrate surface.

In a thin film geometry the typical lateral length scale L_{\parallel} parallel to the substrate surface is much larger than the typical length scale L_{\perp} perpendicular to the substrate surface. In the so-called lubrication approximation for $L_{\perp}/L_{\parallel} \rightarrow 0$ some of these complications can be overcome [33]. This approximation has been used to model thin film flow on topographically [57–62] and chemically [63–65] structured substrates. The disjoining pressure in the vicinity of a substrate surface structure varies on the same small length scale L_{\perp} in normal as well as in lateral direction. Therefore, in the lubrication approximation, the long-ranged lateral variation of the disjoining pressure becomes short-ranged and the lubrication approximation is not suitable for modeling the lateral interaction of a droplet with a substrate structure. However, it has been very successfully used to model the dynamics of liquids on homogeneous substrates [44, 45].

Lattice Boltzmann (LB) simulations have become a very valuable tool for simulating free surface flows [66–70], which has been successfully used to study liquids in contact with structured substrates [71–81]. But although the LB method is often called “mesoscopic” because the free interface between the two fluid phases (between liquid and gas or between two immiscible liquids) is diffuse with a width of a few lattice constants, it is essentially a method to solve macroscopic free interface problems. In most LB simulations of multiphase flows the width of the interface is unphysically large, which, in particular, can influence the dynamics of the three phase contact line. Although it is in principle possible to include arbitrary external potentials, long-ranged intermolecular interactions in the form of an effective interface potential have not been included into the method. One obstacle is the weak but finite compressibility of existing LB methods. In addition, in LB simulations, the material parameters are tightly coupled to the lattice size and to the simulation time step which makes it a nontrivial task to use LB for nanoscale systems.

In phase field methods the free interface is also diffuse. The motion of the free interface is modeled by coupling a phase field which has a value of, e.g., $+1$ in the liquid phase and -1 in the gas phase (alternatively 0 and $+1$) to the Navier Stokes equations [82]. This method has been used to describe the dynamics of droplets [83] and thin films [84–86]. Within the thin film approximation derived from a phase field model also long-ranged intermolecular interactions have been taken into account [87, 88]. However, all the efforts up to now have been targeting homogeneous substrates only.

The linearity of the Stokes equation (7.5) can be used to turn the moving boundary value problem (7.5), (7.7), (7.21), and (7.24) into an integral equation on the surfaces and interfaces surrounding the liquid. Although this method has been successfully used to describe the motion of three-dimensional droplets [89–92], for clarity we focus on the simpler two-dimensional case in the following. With the stream function $\psi(x, z)$, with $u_x = \partial_z \psi$ and $u_z = -\partial_x \psi$, and the vorticity $\varpi = \partial_z u_x - \partial_x u_z$ one can write the Stokes equation (7.5) in its biharmonic form

$$\nabla^4 \psi = 0 \quad \text{and} \quad \nabla^2 \varpi = 0. \quad (7.25)$$

The vorticity and the stream function are coupled via $\nabla^2 \psi = \varpi$. Using the Green's functions to the equations in (7.25) one can write ψ and ϖ inside the liquid as an integral over the surfaces surrounding the liquid [93]. The boundary conditions can also be written in terms of the ψ and ϖ and one obtains a set of equations for the dynamics of the free surface which only involves the values of ψ and ϖ on the surface [94]. Modeling the dynamics of droplets with this scheme requires explicit front tracking, but it is possible to use this method to simulate the dynamics of two-dimensional nanodroplets on structured substrates [2].

All the results on the dynamics of nanodroplets on structured substrates to be discussed below are based on the equilibrium DFT in (7.11) or on linking DFT to hydrodynamics. However, density functionals are not known exactly and the mesoscopic hydrodynamic (7.5), (7.6), (7.7), (7.21), and (7.24) the shear stress σ (see (7.10)) is considered in a local approximation only. In a more consistent description of the dynamics of a liquid on a length scale at which the finite range of intermolecular interactions matters, the non-locality of the stress tensor should be taken into account.

For over-damped Brownian dynamics (a model for the dynamics of suspended colloidal particles) there is a systematic dynamic extension of the equilibrium DFT. This dynamic DFT is based on an equilibrium approximation for the two-particle correlation function [95–97]. Although several attempts towards a dynamical DFT for simple liquids have been made [98, 99], the main obstacle has not been overcome: in liquids the dominant contribution to the viscosity comes from the distortion of the two point correlation function in a shear flow [100, 101] and the equilibrium approximation used for the dynamic DFT for Brownian particles would set this contribution to exactly zero.

Great insight into the molecular structure and dynamics of liquids can be provided by molecular dynamics (MD) simulations [102], i.e., by solving Newton's equations of motion for all atoms in the system. The reason why quantum effects are negligible in most liquids (except for ultra-cold Helium) is that the thermal wavelength $\Lambda = h/\sqrt{2\pi m k_B T}$ (see (7.12)) is smaller than the average distance of the molecules. The molecular dynamics of both free surface liquid flow on chemically [16, 17, 81, 103, 104] and topographically [105–108] structured surfaces has been studied using MD simulations. Although the length scale considered in MD simulations is necessarily on the nanoscale the effect of the long range of dispersion forces on the dynamics of thin films and droplets is ignored in MD simulations.

This is because the range of intermolecular interactions has to be truncated in order to reduce the computational costs. Without truncation each molecule interacts with each other molecule and for N molecules $N(N - 1)$ interaction forces have to be calculated in each time step. If the interaction is truncated (typically at two or three typical molecular distances) the number of force calculations per time step grows only linearly with N and not quadratically.

However, for extremely small systems it might be possible to avoid to truncate the range of interactions. In order to avoid finite size effects one has to keep the gas density low if one wants to keep the number of particles small even in a big simulation box. This can be achieved by considering chain molecules consisting of a few atoms rather than atomic systems [16, 81].

7.3.4 Topographically Structured Substrates

In the vicinity of topographical steps one observes that nanodroplets move laterally [43, 109]. The direction of motion, however, does not depend on the value of the equilibrium contact angle far from the step but on the sign of the Hamaker constant A_H . Near the step shown in Fig. 7.5a nanodroplets move to the left on both sides of the step and in the case shown in Fig. 7.5b to the right, i.e., step up for $A_H > 0$ and step down for $A_H < 0$, respectively. Since the lateral variation of the disjoining pressure is long-ranged, droplets moving away from the step do never stop. However, the droplet velocity decreases rapidly as a function of the distance from the step.

Droplets moving towards the step do not cross it. From the top there is an energy barrier (similar to the Ehrlich–Schwoebel-barrier for an adatom on the terrace of a vicinal crystal surface [110, 111]): to overcome the edge the drop has to deform in such a way that surface area increases which results in an increase of the free energy. This is also true in a macroscopic picture (see Sect. 7.2) or for purely short-ranged interactions. Two-dimensional droplets approaching the step from the bottom stop right in front of the wedge (see Fig. 7.6c) rather than moving into the wedge, although this configuration should represent the global energetic minimum. It is not clear whether this is an artifact of the two-dimensional system or whether there is also a barrier for a three-dimensional droplet. Attempts to directly minimize the droplet free energy in (7.16) using finite element methods [18] (Fig. 7.6a shows a snapshot of an intermediate state of the minimization procedure) have not been conclusive on this respect due to numerical stability problems. However, as shown in Fig. 7.6b, after a rapid initial shape relaxation, during energy minimization the center of mass of the droplet moves in the direction expected for a steepest decent algorithm, i.e., towards the step.

The lateral motion of nanodroplets can be understood as the motion of a droplet on a chemical gradient surface [10, 11] if one defines a “local equilibrium contact angle” by generalizing (7.20) to heterogeneous substrates

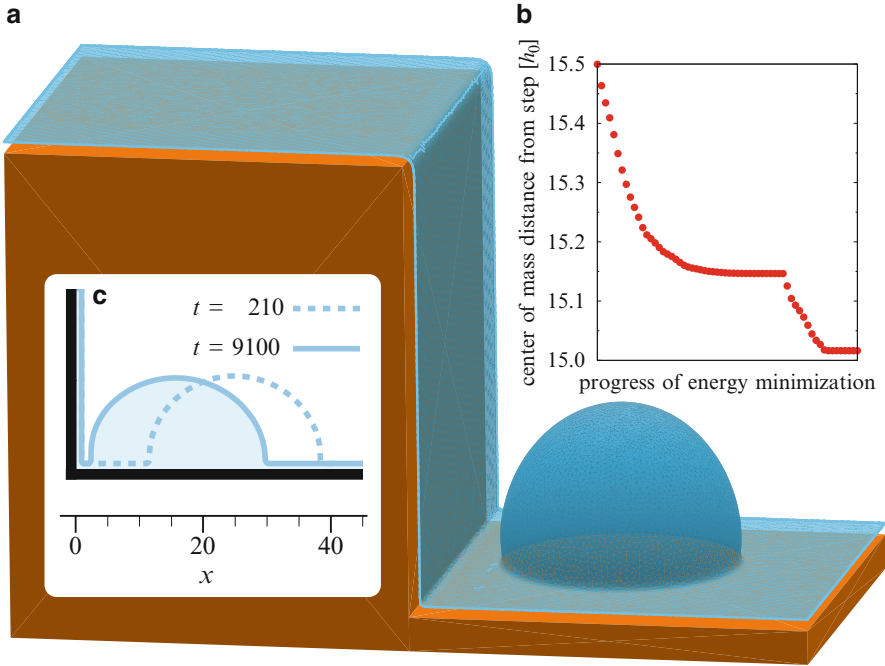


Fig. 7.6 (a) A nanodroplet at the base of a topographic step of height $s = 40h_0$ with $A_H > 0$ and an equilibrium contact angle $\theta_{\text{eq}} = 90^\circ$. The droplet is connected to a wetting film which covers the whole surface. The shape of the droplet was minimized with the SURFACE EVOLVER [18] which uses a steepest decent algorithm. (b) The *inset* shows the horizontal distance of the droplet's center of mass from the step as it evolves in the process of minimization. The position of the droplet has not reached its minimum yet. The existence of an energetic barrier for the droplet to move into the step could not be confirmed or ruled out on the basis of the numerical data. (c) Initial (*dashed line*, after shape relaxation) and final (*full line*) state of a two-dimensional boundary element simulation of a droplet at the base of a very high step with $A_H > 0$ and $\theta_{\text{eq}} = 90^\circ$ [43]

$$\cos \theta_{\text{eq}}(x) = 1 + \int_{h_0(x)}^{\infty} \frac{\Pi(x, z)}{\gamma} dz = 1 + \frac{\omega_{\text{min}}(x)}{\gamma}, \quad (7.26)$$

with $h_0(x)$ defined via $\Pi(x, h_0(x)) = 0$ and $\partial_z \Pi(x, h(x)) < 0$. In other words, $\omega(x, h_0(x)) = \omega_{\text{min}}(x)$ with $\omega_{\text{min}}(x) = \min_{0 < z < \infty} \omega(x, z)$. Figure 7.7 shows $\omega_{\text{min}}(x)$ for the two steps shown in Fig. 7.5. Apart from the immediate vicinity of the step edge, for positive Hamaker constants $\omega_{\text{min}}(x)$ increases from right to left and for negative Hamaker constants $\omega_{\text{min}}(x)$ increases from left to right. In order to calculate the actual value of $\theta_{\text{eq}}(x)$ one further has to specify ω_0/γ . For $\omega_0/\gamma = 1$ one has $\theta_{\text{eq}} = 90^\circ$ far from the step. The resulting position-dependent contact angle is indicated on the right abscissa of Fig. 7.7. Since far from critical points h_0 is a microscopic length (between an Ångström and a nanometer) the equilibrium contact angle changes by a few degrees over a few nanometers, i.e., the gradient of $\theta_{\text{eq}}(x)$ is much larger than on macroscopic chemical gradient surfaces [10]. Therefore it is not surprising to see the nanodroplets migrate.

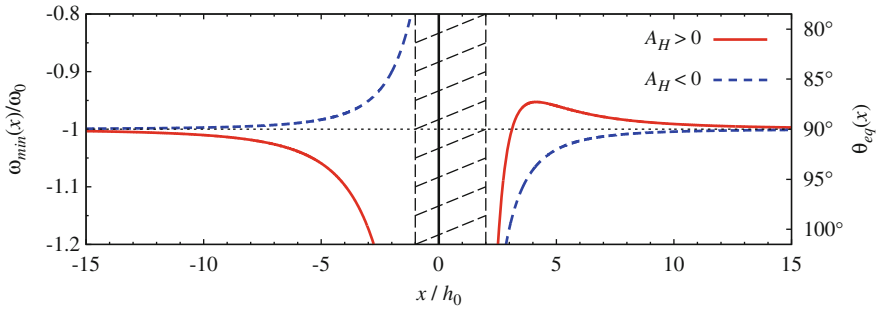


Fig. 7.7 The value of the minimum of $\omega(x, z)$ as a function of z for fixed x plotted vs. x for the cases of $A_H > 0$ (full red line, see Fig. 7.5a) and $A_H < 0$ (dashed blue line, see Fig. 7.5b). The data points between $x/h_0 = -1$ and $x/h_0 = 2$ (shaded region) are not shown since they are too close to the step to be meaningful. The horizontal line indicates the value expected for large distances from the step. An increasing value of $\omega_{\min}(x)$ corresponds to a decreasing value of $\theta_{\text{eq}}(x)$. Therefore $\theta_{\text{eq}}(x)$ increases from left to right for $A_H > 0$ (apart from the interval $2 < x/h_0 < 4.14$) and it decreases for $A_H < 0$. The corresponding values of $\theta_{\text{eq}}(x)$ for a substrate with $\theta_{\text{eq}} = 90^\circ$ (i.e., for $\omega_0/\gamma = 1$) far from the step are given at the right abscissa

For $x > 0$ the curve for $A_H > 0$ has a maximum near $x/h_0 \approx 4$. This corresponds to a minimum of $\theta_{\text{eq}}(x)$. One might be tempted to interpret this as the signature of an energy barrier for a droplet coming from the right. However, this would be an over-interpretation of the simple picture of a step-induced chemical gradient.

Figure 7.6 shows that within the effective interface model, the step edge is covered by a thin wetting film. On partially wetting substrates the thickness of this film can be a nanometer (1.3 nm for molten polystyrene on silicon [44]), but it is usually on the order of an atomic diameter or even less. This means that it is a layer of adsorbed molecules rather than a liquid film. Nevertheless, this wetting film leads to an effective rounding of the step edge. On the nanoscale the three phase contact line is not pinned at the step edge as shown in Fig. 7.2 but it moves continuously around the edge [112]. However, this has only a small effect on the pinning strength of an edge as does macroscopic rounding of the edge.

The situation is different at step edges. As the step height approaches zero, the disjoining pressure (see for example Fig. 7.5) converges steadily to that of a homogeneous flat substrate (for $z > 0$). In this limit the wetting film on the vertical wall ($\alpha = 90^\circ$) of the step (see Fig. 7.6 for a high step) smoothly turns into a horizontal line and the slope of the steepest part of the film smoothly becomes zero. However, this means that the step effectively becomes a step with a slanted wall $\alpha < 90^\circ$ which, according to the macroscopic argument illustrated in Fig. 7.2, pins the three phase contact line much weaker. This is also observed in dewetting experiments on substrates with nanometric steps [113]. In this case the critical step height for pinning of the receding contact line was on the order of the radius of gyration of the polymer molecules. The effective interface model described above results in a similar threshold value for the step height.

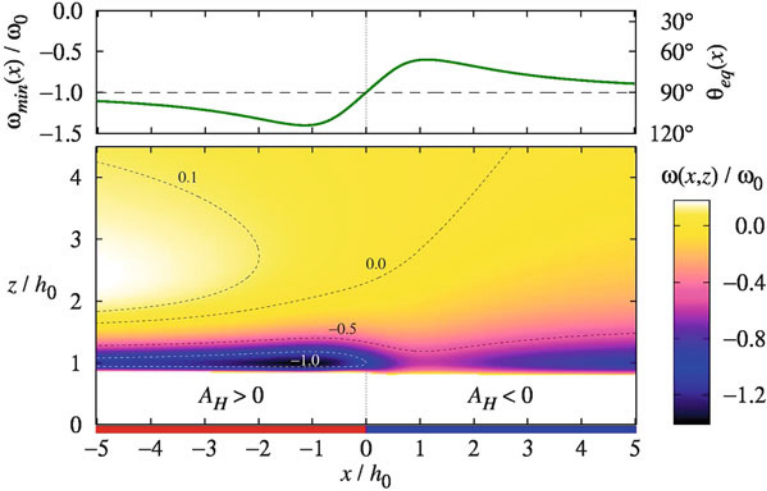


Fig. 7.8 The effective interface potential in the vicinity of a straight chemical step formed by merging two quarter spaces. The *left part* ($x < 0$ and $z < 0$) is made of the material in Fig. 7.5a with $A_H > 0$ and the *right part* ($x > 0$ and $z < 0$) of the material in Fig. 7.5b with $A_H < 0$. ω_0 and therefore θ_{eq} far from the step is equal on both sides. In the *top part* $\omega_{\min}(x)$ is shown (full green line) as well as the asymptotic value far from the step (black dashed line). The corresponding values of $\theta_{\text{eq}}(x)$ for a substrate with $\theta_{\text{eq}} = 90^\circ$ (i.e., for $\omega_0/\gamma = 1$) far from the step are given at the right abszissa

7.3.5 Chemically Structured Substrates

Using the techniques described above it has been shown that nanodroplets in the vicinity of chemical steps exhibit a similar behavior if the step separates two parts of the substrate which consist of different bulk materials [114, 115]. This is the case, e.g., if one cuts a compound material consisting of inclusions embedded in a matrix, or if one fuses two bulk samples and polishes the surface. In these cases, the Hamaker constants differ on the two sides of the step and one gets the same type of long-ranged lateral interaction of the droplet with the step as in the case of the topographic step.

Figure 7.8 shows the effective interface potential in the vicinity of a straight chemical step formed by merging two materials with the same equilibrium contact angle, i.e., $\omega_{\min}(+\infty) = \omega_{\min}(-\infty) = \omega_0$. However, the Hamaker constant on the left side is positive and on the right side it is negative. One can clearly see how the left-hand side influences the effective interface potential on the right-hand side and vice versa. For example, close to the step but on its right hand side $\omega(x,z)$ is positive far from the substrate (i.e., for large z) even though the underlying substrate has a negative Hamaker constant. $\omega_{\min}(x)$ is shown in the upper part of Fig. 7.8. On both sides of the step $\omega_{\min}(x)$ decreases as for increasing x (apart from a narrow region in the direct vicinity of the step). As a consequence, $\theta_{\text{eq}}(x)$ increases from left to right and therefore a nanodroplet moves from right to left. However, coming from the right-hand side, it stops before crossing the step.

In general one observes that nanodroplets move towards the side with the larger Hamaker constant if they start at a certain distance from the step (i.e., if they do not span the step), independent of θ_{eq} far from the step [114]. If the more wettable substrate has a larger Hamaker constant, a droplet starting on the less wettable substrate has a chance to cross the chemical step and move away from the step on the more wettable side. However, whether there is a barrier depends on subtle details.

The direction of motion of nanodroplets spanning the chemical step also depends on the droplet size [115]. For the simple picture of heterogeneity-induced chemical gradient in (7.26) to hold, the droplets have to be so high that the effective interface potential at their apex is negligible. In this case, the energy of a droplet on a substrate with a smaller equilibrium contact angle is smaller than on a substrate with a larger equilibrium contact angle. If the droplet is much smaller this is not necessarily the case. A two-dimensional boundary element simulation of a 5 nm high drop of molten polystyrene (a nonvolatile liquid with a high viscosity such that the dynamics of films and droplets can be observed experimentally [44, 52]) on a silicone substrate with a chemical step formed between two regions covered with silicone oxide layers of different thickness shows that the droplet moves to the side with the larger equilibrium contact angle although the Hamaker constants are equal (they are determined by the silicon substrate).

7.3.6 *Experimental Perspectives*

The dynamics of nanodroplets on structured substrates has not been directly observed yet. One only knows that nanodroplets preferentially condense at topographic steps [116, 117]. One challenge is to prepare suitable substrates, i.e., well-defined topographic and chemical structures. Topographic structures can be produced, e.g., with photolithographic techniques which have been developed for microelectronic devices, and high aspect ratios can be reached. A large number of methods is available for generating a chemical step separating a hydrophilic from a hydrophobic region on a surface (e.g., the boundary between a coated and a non-coated part of the substrate). But in many cases this also leads to a topographic step. However, oxidizing the end groups of self-assembled silane monolayers using the metallic tip of an atomic force microscope allows to prepare well-defined wettability patterns with a 30 nm spatial resolution and with a negligible topographic signature (below 3 Å) [118–120]. The caveat of this method is that only the short-ranged part of the intermolecular interactions is spatially modulated such that the long-ranged lateral interactions between nanodroplets and chemical steps discussed above are negligible in this case.

The main challenge for an experimental verification of the peculiar behavior of nanodroplets at chemical and topographical steps is to prepare and position nanodroplets with nanoscale resolution and then to observe these structures with sufficient spatial and temporal resolution but without influencing them.

Positioning of nanodroplets with nanometer lateral resolution can be achieved with a nano dispenser [121]: the hollow and liquid-loaded tip of an atomic force microscope acts as a pen and allows to deposit droplets with sub-zeptoliter volumes (a cube with 10 nm edge length). Depending of the tip aperture one can reproducibly obtain droplets with diameters down to 70 nm. However, after the transfer of the liquid to the substrate the droplet takes some time to relax its shape [122], and the time scale for this shape relaxation might be comparable to the lateral migration time.

Another option for producing nanodroplets is to pattern a thin film of a material which has a melting point lower than that of the substrate, e.g., by using electron-beam or ion-beam lithography. Regular arrays of islands can be also produced by colloidal monolayer lithography [123]: a densely packed monolayer of colloidal particles is used as a template such that triangular islands form in the gap between three particles. The lateral length scale is controlled by the size of the colloids and islands with an edge length of a few hundred nanometers to a few microns. The volume of the droplets is then controlled by the layer thickness. After annealing the islands turn into nanodroplets. However, as in the case of the nanodispenser the shape relaxation takes time. Melting the islands will speed up shape relaxation but, e.g., for metallic films, the surface tension is so high and the viscosity is so low that inertia comes into play and the droplet actually jump off the substrate [124, 125]. This is an intriguing method for producing nanoparticles but for the purpose of studying the dynamics of nanodroplets this should be avoided.

Nanodroplets are too small to be observed in optical microscopy. X-rays and neutrons are well-established tools for nondestructive structural analysis but scattering methods are hardly suitable for determining the position and shape of an individual droplet and the lack of optical elements limits the resolution of X-ray microscopes. Droplets can be condensed onto surfaces in environmental scanning electron microscopes [126] and they can be observed with high temporal resolution. Spatial resolution of up to a few nanometers is possible but only under optimal conditions and not when imaging soft materials such as droplets.

Scanning probe microscopes have developed into a valuable tool for observing the structure and dynamics of liquid films and droplets (see for example [44, 116, 117]). However, the temporal resolution is fairly low (on the order of minutes, depending on resolution and scan area) and for low viscosity liquids it is difficult to rule out that the tip influences the droplet. However, by quickly freezing the liquid droplet at least the final shape and position of the droplet can be imaged but thermal expansion has to be taken into account.

7.4 Summary and Outlook

Nanodroplets are intriguing objects which behave sometimes in counterintuitive ways—at least this is what theory predicts. These findings are based on static equilibrium DFT and on hydrodynamic equations augmented with features which

are relevant on the nanoscale but which are negligible or summarized into boundary conditions on the macroscopic scale (e.g., the equilibrium contact angle, see Fig. 7.1). These are in particular hydrodynamic slip, thermal fluctuations, and the finite range of intermolecular interactions. Neglecting thermal fluctuations, in the stationary limit these mesoscopic hydrodynamic equations lead to the droplet shapes predicted by the DFT. Most functionals are mean field and thus fluctuation effects, in particular capillary waves, are not included.

While hydrodynamic slip plays an important role for the dynamics of the liquid within a moving three phase contact line, it is not to be expected that it changes the qualitative behavior of nanodroplets as this is driven predominantly by the energetics. And it has been shown that the same is true for thermal fluctuations, although they might help to overcome pinning. The main player are the long-ranged dispersion forces. On homogeneous substrates they are summarized into the effective interface potential $\omega(z)$ (see Fig. 7.4) which also determines the equilibrium wetting behavior of the system. On heterogeneous substrates the effective interface potential (see Fig. 7.8 for a chemical step) as well as its derivative with respect to the film thickness, i.e., the disjoining pressure Π (see Fig. 7.5 for a topographic step) depend on the lateral coordinates as well. This leads to a lateral force on a nanodroplet. The sign of this force depends only on the sign of the Hamaker constant A_H and at a topographic step nanodroplets are expected to move in the step-up direction for $A_H > 0$ (see Fig. 7.6) and in step-down direction for $A_H < 0$.

At a chemical step the droplets should move towards the side with the larger Hamaker constant. This can be understood if one interprets the lateral variation of the effective interface potential as an effective chemical gradient, i.e., a laterally varying equilibrium contact angle (see Fig. 7.7 for a topographic step and Fig. 7.8 for a chemical step). The behavior at chemical steps is particularly intriguing as it is independent of the equilibrium contact angles far from the step: it can happen that the droplet moves towards the less wettable side. However, in this case it does not cross the step. In particular at chemical steps there is also a strong size dependence. While the free energy of a macroscopic droplet is always smaller on the side with the smaller equilibrium contact angle, for extremely small droplets the situation can be reversed (for an example see Fig. 7.9).

Since this peculiar behavior of nanodroplets is driven by free energy gradients, it is not specific to liquids. Molecular dynamics simulations of gold clusters on graphite with steps show a strong interaction of the step edges with the clusters, but the interactions are purely short-ranged and the steps were only one atom high [127]. On substrates with higher steps and for non-metallic clusters the same phenomena discussed above should be observable.

The development of experimental techniques will determine whether the peculiar dynamics of nanodroplets on structured substrates will ever be observed directly. Maybe clusters are better candidates since they can be studied under high vacuum and in clean conditions on atomically smooth surfaces. However, understanding nanofluidics will be more and more important in order to push the progressive miniaturization of microelectronic, micromechanical, and microfluidic devices even further.

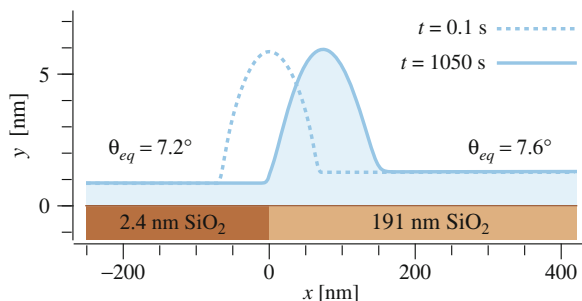


Fig. 7.9 2D boundary element simulation of a small nanodroplet (apex height lower than 7.5 nm) at the chemical step between a silicon substrate with a thin and a thick oxide layer [115]. The Hamaker constant is equal on both sides. Shown are the initial (*dashed line*) and final (*full line*) position of the droplet. Larger droplets move to the *left*

Acknowledgements Markus Rauscher thanks S. Dietrich for supporting this research. The SURFACE EVOLVER calculations were performed by D. Maier and H. Bartsch in their bachelor thesis project.

References

1. Rauscher, M., Dietrich, S.: *Ann. Rev. Mater. Res.* **38**, 143 (2008)
2. Rauscher, M., Dietrich, S.: *Soft Matter* **5**(16), 2997 (2009)
3. Rauscher, M., Dietrich, S.: In: Sattler, K.D. (ed.) *Handbook of Nanophysics*, vol. I: Principles and Methods, chap. 11, pp. 1–23. CRC, Boca Raton (2010)
4. Dietrich, S., Rauscher, M., Napiórkowski, M.: In: Ondarçuhu, T., Aimé, J.P. (eds.) *Nanoscale Liquid Interfaces: Wetting, Patterning and Force Microscopy at Molecular Scale*. Pan Stanford Publishing, Singapore (2012)
5. de Gennes, P.G.: *Rev. Mod. Phys.* **57**(3), 827 (1985)
6. Dietrich, S.: In: Domb, C., Lebowitz, J.L. (eds.) *Phase Transitions and Critical Phenomena*, vol. 12, Chap. 1, pp. 1–218. Academic, London (1988)
7. de Gennes, P.G., Brochard-Wyart, F., Quéré, D.: *Capillarity and Wetting Phenomena: Drops, Bubbles, Pearls, Waves*. Springer, New York (2004)
8. Ondarçuhu, T., Veyssié, M.: *J. Phys. II France* **1**(1), 75 (1991)
9. Ondarçuhu, T., Raphaël, E.: *C. R. Acad. Sci. Paris II* **314**, 453 (1992)
10. Chaudhury, M.K., Whitesides, G.M.: *Science* **256**(5063), 1539 (1992)
11. Pismen, L.M., Thiele, U.: *Phys. Fluids* **18**(4), 042104 (2006)
12. Moosavi, A., Mohammadi, A.: *J. Phys. Condens. Matter* **23**(11), 085004 (2011)
13. Brinkmann, M., Lipowsky, R.: *J. Appl. Phys.* **92**(8), 4296 (2002)
14. Lipowsky, R., Brinkmann, M., Dimova, R., Franke, T., Kierfeld, J., Zhand, X.: *J. Phys. Condens. Matter* **17**(9), S537 (2005)
15. Dietrich, S., Popescu, M.N., Rauscher, M.: *J. Phys. Condens. Matter* **17**(9), S577 (2005)
16. Koplik, J., Lo, T.S., Rauscher, M., Dietrich, S.: *Phys. Fluids* **18**(3), 032104 (2006)
17. Rauscher, M., Dietrich, S., Koplik, J.: *Phys. Rev. Lett.* **98**(22), 224504 (2007)
18. Brakke, K.: *Exp. Math.* **1**(2), 141 (1992)
19. Bico, J., Thiele, U., Quéré, D.: *Colloids Surf. A Physicochem. Eng. Aspects* **206**(1–3), 41 (2002)

20. Lafuma, A., Quéré, D.: *Nat. Mater.* **2**(7), 457 (2003)
21. Quéré, D.: *Rep. Prog. Phys.* **68**, 2495 (2005)
22. Quéré, D.: *Ann. Rev. Mater. Res.* **38**, 71 (2008)
23. Yao, Z., Bowick, M.J.: *Soft Matter* **8**(4), 1142 (2012)
24. Seemann, M., Brinkmann, R., Kramer, F.F., Lange, E.J., Lipowsky, R.: *Proc. Natl. Acad. Sci. USA* **102**(6), 1848 (2005)
25. Khare, K., Herminghaus, S., Baret, J.C., Law, B.M., Brinkmann, M., Seemann, R.: *Langmuir* **23**(26), 12997 (2007)
26. Herminghaus, S., Brinkmann, M., Seemann, R.: *Ann. Rev. Mater. Res.* **38**, 101 (2008)
27. Gibbs, J.W.: *The Scientific Papers of J. Willard Gibbs*, vol. I: Thermodynamics, chap. III, pp. 55–353. Longmans, Green, London (1906)
28. Oliver, J.F., Hu, C., Mason, S.G.: *J. Colloid Interface Sci.* **59**(3), 568 (1977)
29. Morison, K.R., Sellier, M.: *Int. J. Multiphase Flow* **39**, 245 (2012)
30. Delmas, M., Monthieux, M., Ondarçuhu, T.: *Phys. Rev. Lett.* **106**(13), 136102 (2011)
31. Eral, H.B.B., de Ruitter, J., de Ruitter, R., Oh, J.M., Semprebon, C., Brinkman, M., Mugele, F.: *Soft Matter* **7**(11), 5138 (2011)
32. Lauga, E., Brenner, M.P., Stone, H.A.: In: Tropea, C., Yarin, A.L., Foss, J.F. (eds.) *Springer Handbook of Experimental Fluid Mechanics*, chap. Part C, pp. 1219–1240. Springer, Berlin, (2007)
33. Oron, A., Davis, S.H., Bankoff, S.G.: *Rev. Mod. Phys.* **69**(3), 931 (1997)
34. Ralston, J., Popescu, M., Sedev, R.: *Ann. Rev. Mater. Res.* **38**, 23 (2008)
35. Hansen, J.P., McDonald, I.R.: *Theory of Simple Liquids*, 2nd edn. Academic, London (1990)
36. Evans, R.: *Adv. Phys.* **28**(2), 143 (1979)
37. Percus, J.K.: *J. Stat. Phys.* **15**(6), 505 (1976)
38. Roth, R., Evans, R., Lang, A., Kahl, G.: *J. Phys. Condens. Matter* **14**(46), 12063 (2002)
39. Hansen-Goos, H., Roth, R.: *J. Phys. Condens. Matter* **18**(37), 8413 (2006)
40. Napiórkowski, M., Dietrich, S.: *Phys. Rev. E* **47**(3), 1836 (1993)
41. Robbins, M.O., Andelman, D., Joanny, J.F.: *Phys. Rev. A* **43**(8), 4344 (1991)
42. Dietrich, S., Napiórkowski, M.: *Phys. Rev. A* **43**(4), 1861 (1991)
43. Moosavi, A., Rauscher, M., Dietrich, S.: *J. Phys. Condens. Matter* **21**(46), 464120 (2009)
44. Becker, J., Grün, G., Seemann, R., Mantz, H., Jacobs, K., Mecke, K.R., Blossey, R.: *Nat. Mater.* **2**(1), 59 (2003)
45. Neto, C., Jacobs, K., Seemann, R., Blossey, R., Becker, J., Grün, G.: *J. Phys. Condens. Matter* **15**(19), 3355 (2003)
46. Landau, L.D., Lifshitz, E.M.: *Fluid Mechanics, Course of Theoretical Physics*, vol. 6, 2nd edn. Elsevier, Amsterdam (2005)
47. Mashiyama, K.T., Mori, H.: *J. Stat. Phys.* **18**(4), 385 (1978)
48. Forster, D., Nelson, D.R., Stephen, M.J.: *Phys. Rev. Lett.* **36**(15), 867 (1976)
49. Forster, D., Nelson, D.R., Stephen, M.J.: *Phys. Rev. A* **16**(2), 732 (1977)
50. Hohenberg, P.C., Swift, J.B.: *Phys. Rev. A* **46**(8), 4773 (1992)
51. Swift, J.B., Babcock, K.L., Hohenberg, P.C.: *Physica A* **204**(1–4), 625 (1994)
52. Fetzer, R., Rauscher, M., Seemann, R., Jacobs, K., Mecke, K.: *Phys. Rev. Lett.* **99**(11), 114503 (2007)
53. Mecke, K., Falk, K., Rauscher, M.: In: Radons, G., Rumpf, B., Schuster, H.G. (eds.) *Nonlinear Dynamics of Nanosystems*, pp. 121–142. Wiley-VCH, Berlin (2010)
54. Blossey, R., Münch, A., Rauscher, M., Wagner, B.: *Eur. Phys. J. E* **20**(3), 267 (2006)
55. Rauscher, M., Blossey, R., Münch, A., Wagner, B.: *Langmuir* **24**(21), 12290 (2008)
56. Münch, A., Wagner, B.: *J. Phys. Condens. Matter* **23**(18), 184101 (2011)
57. Kalliadasis, S., Homsy, G.M.: *J. Fluid Mech.* **448**, 387 (2001)
58. Bielarz, C., Kalliadasis, S.: *Phys. Fluids* **15**(9), 2512 (2003)
59. Savva, N., Kalliadasis, S.: *Phys. Fluids* **21**(9), 092102 (2009)
60. Gaskell, P.H., Jimack, P.K., Sellier, M., Thompson, H.M., Wilson, M.C.T.: *J. Fluid Mech.* **509**, 253 (2004)
61. Gaskell, P.H., Jimack, P.K., Sellier, M., Thompson, H.M.: *Phys. Fluids* **18**(1), 013601 (2006)

62. Baxter, S.J., Power, H., Cliffe, K.A., Hibberd, S.: *Phys. Fluids* **21**(3), 032102 (2009)
63. Kondic, L., Diez, J.A.: *Colloids Surf. A Physicochem. Eng. Aspects* **214**(1–3), 1 (2003)
64. Kondic, L., Diez, J.: *Phys. Fluids* **16**(9), 3341 (2004)
65. Mechkov, S., Rauscher, M., Dietrich, S.: *Phys. Rev. E* **77**(6), 061605 (2008)
66. Shan, X., Chen, H.: *Phys. Rev. E* **47**(3), 1815 (1993)
67. Shan, X., Chen, H.: *Phys. Rev. E* **49**(4), 2941 (1994)
68. Swift, M.R., Osborn, W.R., Yeomans, J.M.: *Phys. Rev. Lett.* **75**(5), 830 (1995)
69. Swift, M.R., Orlandini, E., Osborn, W.R., Yeomans, J.M.: *Phys. Rev. E* **54**(5), 5041 (1996)
70. Langaas, K., Yeomans, J.M.: *Eur. Phys. J. B* **15**, 133 (2000)
71. Léopoldès, J., Dupuis, A., Bucknall, D.G., Yeomans, J.M.: *Langmuir* **19**(23), 9818 (2003)
72. Kuksenok, O., Jasnow, D., Yeomans, J., Balazs, A.C.: *Phys. Rev. Lett.* **91**(10), 108303 (2003)
73. Dupuis, A., Yeomans, J.M.: In: Bubak, M., van Albada, G.D., Sloot, P.M.A., Dongarra, J.J. (eds.) *Computational Science - ICCS 2004. Lecture Notes in Computer Science*, vol. 3039, pp. 556–563. Springer, Berlin (2004). [dx.doi.org/10.1007/b98005](https://doi.org/10.1007/b98005). *Cond-mat/0401150*
74. Dupuis, A., Léopoldès, J., Bucknall, D.G., Yeomans, J.M.: *Appl. Phys. Lett.* **87**(2), 024103 (2005)
75. Dupuis, A., Yeomans, J.M.: *Langmuir* **21**(6), 2624 (2005)
76. Kusumaatmaja, H., Léopoldès, J., Dupuis, A., Yeomans, J.M.: *Europhys. Lett.* **73**(5), 740 (2006)
77. Kusumaatmaja, H., Yeomans, J.: *Langmuir* **23**(2), 956 (2007)
78. Kusumaatmaja, H., Yeomans, J.M.: *Langmuir* **23**(11), 6019 (2007)
79. Hyväluoma, J., Harting, J.: *Phys. Rev. E* **100**(24), 246001 (2008)
80. Harting, J., Kunert, C., Hyväluoma, J.: *Microfluid Nanofluid* **8**(1), 1 (2009)
81. Dörfler, F., Rauscher, M., Koplik, J., Harting, J., Dietrich, S.: *Soft Matter* **8**(35), 9221 (2012)
82. Jacqmin, D.: *J. Comp. Phys.* **155**, 96 (1999)
83. Ding, H., Spelt, P.D.M.: *Phys. Rev. E* **75**(4), 046708 (2007)
84. Pismen, L.M., Pomeau, Y.: *Phys. Rev. E* **62**(2), 2480 (2000)
85. Thiele, U., Velarde, M.G., Neuffer, K., Pomeau, Y.: *Phys. Rev. E* **64**(3), 031602 (2001)
86. Thiele, U., Velarde, M.G., Neuffer, K., Bestehorn, M., Pomeau, Y.: *Phys. Rev. E* **64**(6), 061601 (2001)
87. Pismen, L.M.: *Phys. Rev. E* **64**(2), 021603 (2001)
88. Pismen, L.M.: *Colloids Surf. A Physicochem. Eng. Aspects* **206**(1–3), 11 (2002)
89. Dimitrakopoulos, P., Higdon, J.J.L.: *J. Fluid Mech.* **336**, 351 (1997)
90. Dimitrakopoulos, P., Higdon, J.J.L.: *J. Fluid Mech.* **377**, 189 (1998)
91. Dimitrakopoulos, P., Higdon, J.J.L.: *J. Fluid Mech.* **435**, 327 (2001)
92. Dimitrakopoulos, P.: *J. Fluid Mech.* **580**, 451 (2007)
93. Kelmanson, M.A.: *J. Comp. Phys.* **51**, 139 (1983)
94. Mazouchi, A., Gramlich, C.M., Homsy, G.M.: *Phys. Fluids* **16**(5), 1647 (2004)
95. Marconi, U.M.B., Tarazona, P.: *J. Chem. Phys.* **110**(16), 8032 (1999)
96. Marconi, U.M.B., Tarazona, P.: *J. Phys. Condens. Matter* **12**(8A), A413 (2000)
97. Archer, A.J., Rauscher, M.: *J. Phys. A Math. Gen.* **37**(40), 9325 (2004)
98. Archer, A.J.: *J. Phys. Condens. Matter* **18**(24), 5617 (2006)
99. Marconi, U.M.B., Melchionna, S.: *J. Chem. Phys.* **131**(1), 014105 (2009)
100. Green, H.S.: *The Molecular Theory of Fluids*. North-Holland, Amsterdam (1952)
101. Kreuzer, H.J.: *Nonequilibrium Thermodynamics and Its Statistical Foundations*. Clarendon, Oxford (1981)
102. Frenkel, D., Smit, B.: *Understanding Molecular Simulation*, 2nd edn. Academic, San Diego (2002)
103. Yaneva, J., Milchev, A., Binder, K.: *J. Chem. Phys.* **121**(24), 12632 (2004)
104. Cieplak, M., Koplik, J., Banavar, J.R.: *Phys. Rev. Lett.* **96**(11), 114502 (2006)
105. Cottin-Bizonne, C., Barrat, J.L., Bocquet, L., Charlaix, E.: *Nat. Mater.* **2**(4), 237 (2003)
106. Cottin-Bizonne, C., Barentin, C., Charlaix, E., Bocquet, L., Barrat, J.L.: *Eur. Phys. J. E* **15**, 427 (2004)
107. Cao, B.Y., Chen, M., Guo, Z.Y.: *Phys. Rev. E* **74**(6), 066311 (2006)

108. Huang, D.M., Cottin-Bizonne, C., Ybert, C., Bocquet, L.: *Phys. Rev. Lett.* **06**, 064503 (2008)
109. Moosavi, A., Rauscher, M., Dietrich, S.: *Phys. Rev. Lett.* **97**(23), 236101 (2006)
110. Ehrlich, G., Hudde, F.G.: *J. Chem. Phys.* **44**(3), 1039 (1966)
111. Schwoebel, R.L., Shipsey, E.J.: *J. Appl. Phys.* **37**(10), 3682 (1966)
112. Dutka, F., Napiórkowski, M., Dietrich, S.: *J. Chem. Phys.* **136**(6), 064702 (2012)
113. Ondarçuhu, T., Piednoir, A.: *Nano Lett.* **5**(9), 1744 (2005)
114. Moosavi, A., Rauscher, M., Dietrich, S.: *Langmuir* **24**(3), 734 (2008)
115. Moosavi, A., Rauscher, M., Dietrich, S.: *J. Chem. Phys.* **129**(4), 044706 (2008)
116. Hu, J., Xiao, X.D., Salmeron, M.: *Appl. Phys. Lett.* **67**(4), 476 (1995)
117. Hu, J., Carpick, R.W., Salmeron, M., Xiao, X.D.: *J. Vac. Sci. Tech. B* **14**(2), 1341 (1996)
118. Checco, A., Gang, O., Ocko, B.M.: *Phys. Rev. Lett.* **96**(5), 056104 (2006)
119. Checco, A., Schollmeyer, H., Daillant, J., Guenoun, P., Boukherroub, R.: *Langmuir* **22**(1), 116 (2006)
120. Checco, A.: *Phys. Rev. Lett.* **102**(10), 106103 (2009)
121. Fang, A., Dujardin, E., Ondarçuhu, T.: *Nano Lett.* **6**(10), 2368 (2006)
122. Fabi/e, L., Ondarçuhu, T.: *Soft Matter* **8**(18), 4995 (2012)
123. Burmeister, F., Badowsky, W., Braun, T., Wieprich, S., Boneberg, J., Leiderer, P.: *Appl. Surf. Sci.* **144–145**, 461 (1999)
124. Habenicht, A., Olapinski, M., Burmeister, F., Leiderer, P., Boneberg, J.: *Science* **309**(5743), 2043 (2005)
125. Boneberg, J., Habenicht, A., Benner, D., Leiderer, P., Trautvetter, M., Pfahler, C., Plettl, A., Ziemann, P.: *Appl. Phys. A* **93**(2), 415 (2008)
126. Stokes, D.J.: *Adv. Eng. Mater.* **3**(2), 126 (2001)
127. Yoon, B., Luedtke, W.D., Gao, J., Landman, U.: *J. Phys. Chem. B* **107**(24), 5882 (2003)